Smooth Quantum Hydrodynamic Model vs. NEMO Simulation of a Resonant Tunneling Diode

Carl L. Gardner* and Christian Ringhofer*
Department of Mathematics
Arizona State University
Tempe, AZ 85287-1804

Gerhard Klimeck† and R. Chris Bowen†
High Performance Computing Systems and Applications Group
Jet Propulsion Laboratory
California Institute of Technology
Pasadena, CA 91109

Keywords: resonant tunneling diode, quantum hydrodynamic model.

Abstract

The "smooth" quantum hydrodynamic (QHD) model is an extension of the classical hydrodynamic model for semiconductor devices which can handle in a mathematically rigorous way the discontinuities in the classical potential energy which occur at heterojunction barriers in quantum semiconductor devices. Smooth QHD model simulations of the current-voltage curve of a resonant tunneling diode

*Research supported in part by the National Science Foundation under grant DMS-9706792.

†The NEMO work described here was carried out by the Jet Propulsion Laboratory, California Institute of Technology under a contract with the National Aeronautics and Space Administration.

are presented which exhibit negative differential resistance—the experimental signal for quantum resonance effects—and are compared with the experimentally verified current-voltage curves predicted by the simulator NEMO.

1 Smooth QHD Model Simulations

Quantum transport effects including electron or hole tunneling through potential barriers and charge buildup in quantum wells can be incorporated into the hydrodynamic description of charge propagation in semiconductor devices. Refs. [1] and [2] present an extension of the classical hydrodynamic model which can handle in a mathematically rigorous way the discontinuities in the classical potential energy which occur at heterojunction barriers in quantum semiconductor devices. This "smooth" quantum hydrodynamic (QHD) model is valid to all orders of $\hbar^2/(mT_0l^2)$ (where m is the effective mass of electrons or holes, T_0 is the ambient temperature, and l is a typical length scale for the problem) and to first order in the classical potential energy.

The smooth QHD equations have the same form as the classical hydrodynamic equations:

$$\frac{\partial n}{\partial t} + \frac{\partial}{\partial x_i}(nu_i) = 0 \tag{1}$$

$$\frac{\partial}{\partial t}(mnu_j) + \frac{\partial}{\partial x_i}(mnu_iu_j - P_{ij}) = -n\frac{\partial V}{\partial x_j} - \frac{mnu_j}{\tau_p} \tag{2}$$

$$\frac{\partial W}{\partial t} + \frac{\partial}{\partial x_i}(u_iW - u_jP_{ij} + q_i) = -nu_i\frac{\partial V}{\partial x_i} - \frac{\left(W - \frac{3}{2}nT_0\right)}{\tau_w} \tag{3}$$

where n is the electron density, u_i is the velocity, m is the effective electron mass, P_{ij} is the stress tensor, V is the potential energy, W is the energy density, and q_i is the heat flux. Boltzmann's constant k_B is set equal to 1. Indices i, j equal 1, 2, 3, and repeated indices are summed over. Electron scattering is modeled by the standard relaxation time approximation, with momentum and energy relaxation times τ_p and τ_w.

The stress tensor and energy density are

$$P_{ij} = -nT\delta_{ij} - \frac{\hbar^2 n}{4mT_0}\frac{\partial^2 \overline{V}}{\partial x_i \partial x_j} \tag{4}$$

$$W = \frac{3}{2}nT + \frac{1}{2}mnu^2 + \frac{\hbar^2 n}{8mT_0}\nabla^2\overline{V} \tag{5}$$

where T is the temperature of the electron gas and the "quantum" potential $\overline{V}$ is given by ($\beta = 1/T_0$)

$$\overline{V}(\beta, \mathbf{x}) = \int_0^\beta \frac{d\beta'}{\beta}\left(\frac{\beta'}{\beta}\right)^2 \int d^3x' \left(\frac{2m\beta}{\pi(\beta-\beta')(\beta+\beta')\hbar^2}\right)^{3/2} \times$$

$$\exp\left\{-\frac{2m\beta}{(\beta-\beta')(\beta+\beta')\hbar^2}(\mathbf{x}'-\mathbf{x})^2\right\} V(\mathbf{x}'). \tag{6}$$

The heat flux

$$\mathbf{q} = -\kappa\nabla T - \frac{\hbar^2 n}{8m}\nabla^2\mathbf{u} \tag{7}$$

incorporates both classical and quantum effects and is derived in Ref. [3] by a Chapman-Enskog expansion. The quantum contribution to the heat flux is necessary for internal consistency of the QHD model.

We model the relaxation times τ_p and τ_w by modified Baccarani-Wordeman models

$$\tau_p = m\mu_{n0}\frac{T_0}{T}, \quad \tau_w = \frac{\tau_p}{2}\left(1 + \frac{\frac{3}{2}T}{\frac{1}{2}mv_s^2}\right) \tag{8}$$

and the coefficient κ by

$$\kappa = \kappa_0\mu_{n0}nT_0 \tag{9}$$

where μ_{n0} is the low-field electron mobility, v_s is the electron saturation velocity, and $\kappa_0 > 0$ is a phenomenological constant.

The transport equations (1)–(3) are coupled to Poisson's equation for the electrostatic potential energy

$$\nabla\cdot(\epsilon\nabla V_P) = e^2(N-n) \tag{10}$$

where ϵ is the dielectric constant, $e > 0$ is the electronic charge, and N is the density of donors. The total potential energy V consists of two parts, one from Poisson's equation V_P and the other from the potential barriers V_B:

$$V = V_B + V_P. \tag{11}$$

V_B has a step function discontinuity at potential barriers.

To derive the stress tensor and energy density, we constructed a "quantum Maxwellian" density matrix as an $O(\beta V)$ solution to the Bloch equation.

Then using the momentum-shifted quantum Maxwellian, we took moments of the quantum Liouville equation to derive the smooth QHD equations [1].

There are two contributions to the quantum potential $\overline{V}$: the double barrier potential and the "self-consistent" electrostatic potential from Poisson's equation. Note that second derivatives of $\overline{V}$ appear in the stress tensor and energy density, which then are differenced in the smooth QHD transport equations. Thus we compute

$$\overline{V}'' = \overline{V}''_B + \overline{V}''_P. \tag{12}$$

$\overline{V}''_B$ is just computed once since it only depends on the barriers and not on the applied voltage or state variables (n, u, T, V_P). In computing $\overline{V}''_P$, we first use Poisson's equation to obtain

$$\overline{V}''_P(\beta, x) = \frac{e^2}{\epsilon} \int_0^\beta \frac{d\beta'}{\beta} \left(\frac{\beta'}{\beta}\right)^2 \int dx' \left(\frac{2m\beta}{\pi(\beta-\beta')(\beta+\beta')\hbar^2}\right)^{3/2} \times$$

$$\exp\left\{-\frac{2m\beta}{(\beta-\beta')(\beta+\beta')\hbar^2}x'^2\right\} \left(N(x'+x) - n(x'+x)\right). \tag{13}$$

The convolution (13) can be computed efficiently using discrete Fourier transform algorithms.

We simulate a GaAs resonant tunneling diode with $Al_{0.3}Ga_{0.7}As$ double barriers at 300 K. The barrier height is equal to 280 meV. The diode consists of n^+ source (at the left) and drain (at the right) regions with the doping density $N = 10^{18}$ cm^{-3}, and an n channel with $N = 5 \times 10^{15}$ cm^{-3}. The channel is 200 Å long, the barriers are 25 Å wide, and the quantum well between the barriers is 50 Å wide. Note that the device has 50 Å spacers between the barriers and the contacts.

In Fig. 1, the experimental signal of quantum resonance—negative differential resistance (NDR), a region of the current-voltage (I-V) curve where the current *decreases* as the applied voltage is increased—is displayed for the smooth QHD model.

2 NEMO Simulations

The need for a resonant tunneling device modeling tool prompted a device modeling project at the Central Research Laboratory of Texas Instruments

(which transferred to Raytheon Systems in 1997). NEMO was developed as a general purpose quantum mechanics based 1D device design and analysis tool from 1993–97. The tool is available to US researchers by request on the NEMO web site [9]. NEMO is based on the non-equilibrium Green function approach, which allows a fundamentally sound inclusion of the required physics: band structure, scattering, and charge self-consistency. The theoretical approach is documented in Refs. [10, 11] while some of the major simulation results are documented in Refs. [12, 13, 14, 15, 16, 17]. NEMO development is presently continued at the Jet Propulsion Laboratory towards the modeling of light detection and emission devices.

The structure under consideration in this paper has been simulated using NEMO as well. The central resonant tunneling diode (RTD) is described by 9 monolayer $\approx$ 2.5 nanometer $Al_{0.3}Ga_{0.7}As$ barriers and a 18 monolayer $\approx$ 5.1 nanometer GaAs well. It is clad symmetrically by 18 monolayers of low doping GaAs spacer of 5×10^{15} cm^{-3} and 30 nanometer high doping contacts of 10^{18} cm^{-3}. The four NEMO simulations shown here in Fig. 2 are based on three different band structure models: (1) single band effective mass model, $m_{GaAs} = 0.067\ m_e$, $m_{AlGaAs} = 0.081\ m_e$, and $\Delta E_c = 284$ meV, (2) single band effective mass model with $m_{GaAs} = m_{AlGaAs} = 0.07\ m_e$, (3) two band $k \cdot p$ with the parameters in (1) plus energy gaps $\Delta E_{GaAs} = 1.424$ eV and $\Delta E_{AlGaAs} = 1.846$ eV, and (4) a ten band sp3s* with $\Delta E_c = 284$ meV. The potential in these simulations is based on a self-consistent Hartree potential and includes the exchange energy within the LDA assumption.

The current-voltage characteristics based on the 2 band and 10 band simulations appear a little more rounded close to the voltage peak at 0.15–0.25 V compared to the single band simulation due to the full band numerical transverse momentum integration performed in these two models. The single band simulation is based on an analytic transverse momentum integration (Tsu-Esaki) which neglects the different dispersions in the emitter potential notch and the central RTD. Details of the effects of numerical transverse momentum integration have been previously discussed in detail in Ref. [14].

The I-V peak position occurs roughly when the central RTD resonance is lowered under the emitter subband by the applied bias. At zero bias the central resonance is predicted at approximately 105–108 meV for all three band models. That energy includes a built-in potential of about 30 meV above the contact band edge due to the low doping in the central region. Assuming a semiclassical charge distribution in the contacts and zero charge in the central RTD, NEMO predicts a current peak at about 0.21 V (not

shown here). Including Hartree self-consistency linearizes the I-V curve and pushes the peak to a higher voltage [12, 14] at 0.25 V.

The four simulations differ mostly in the current density of the current voltage peak at about 0.25 V and the higher voltage turn-on. The higher current amplitude can be understood with arguments presented in Ref. [14] where the imaginary bands in the AlGaAs barriers connect the conduction to the valence band in the multiband models, thereby decreasing the wave decay constant in the barrier compared to the single band model. The band wrapping is stronger in the 10 band model than the 2 band model due to the additional valence bands and spin-orbit coupling present in the more complete 10 band model. The increased valley current and earlier turn-on in the valley current can be explained by a similar argument as well as an increased influence of band non-parabolicity in the GaAs as the voltage is increased and higher energies are probed in the GaAs.

All four NEMO simulations do not treat any scattering inside the RTD explicitly. We have found for high performance, high current density RTDs, that at room temperature scattering effects due to polar optical phonons, acoustic phonons and interface roughness [15, 16, 17] are negligible compared to the first order band structure effects such as band wrapping and band non-parabolicity. The aluminum content of the barrier material in this structure is small enough and the barriers are thin enough that X states cannot influence the current flow significantly. The valley current in this structure is entirely due to thermionic transport through the second RTD state. Scattering is included in the contacts (not the central RTD) through a relaxation rate approximation through an optical potential of 1 meV [12].

The three different band structure models predict a peak current and voltage that is close enough for all experimental/practical design purposes *for this particular structure*. We explicitly note that this cannot be generalized for all structures in the GaAs/AlGaAs material system, but it is due here to the small barrier thicknesses. The predictions of the valley current and the diode turn-on differ already significantly as discussed above. However, for the simple exploration of the capabilities of the quantum hydrodynamic model it is therefore justified to utilize a single band effective mass model.

3 Comparison and Conclusion

If we view the RTD NEMO simulations as an experimentally verified standard, we conclude that the hydrodynamic model predicts a current density that is in excellent agreement but with a peak voltage that is too low, primarily due to the fact that the hydrodynamic approximation only allows the electrons in the drain to cool to near ambient temperature over a length scale on the order of 100 nanometers (see Fig. 3). However the hydrodynamic simulations do predict a negative differential resistance region which will surprise many readers.

The particular structure of thin and shallow $Al_{0.3}Ga_{0.7}As$ barriers chosen here results in a large current density that is close to the very best current densities (300–800 kA/cm^2) that have been achieved experimentally in the InP material system. Such high current densities are typically not achieved in the GaAs system considered here. A current density of 300 kA/cm^2 at a voltage of 0.25 V corresponds to a resistance of $8.3 \times 10^{-7} \Omega/\text{cm}^2$ which is close to world class contact resistances that can be achieved in the GaAs material system. This implies that the structure simulated in this paper would suffer from a large series resistance effect due to the alloyed contacts which cannot be accounted for by scattering or mobility type simulations in the high doping regions. It is noted that the target of this investigation is not to design a better GaAs/AlGaAs RTD, but to present a quantum hydrodynamic simulation of an RTD that roughly compares to a NEMO simulation.

References

[1] C. L. Gardner and C. Ringhofer, "Smooth quantum potential for the hydrodynamic model," *Physical Review E*, vol. 53, pp. 157–167, 1996.

[2] C. L. Gardner and C. Ringhofer, "Approximation of thermal equilibrium for quantum gases with discontinuous potentials and application to semiconductor devices," *SIAM Journal on Applied Mathematics*, vol. 58, pp. 780–805, 1998.

[3] C. L. Gardner and C. Ringhofer, "The Chapman-Enskog expansion and the quantum hydrodynamic model for semiconductor devices," *VLSI Design*, vol. 10, pp. 415–435, 2000.

[4] H. L. Grubin, T. R. Govindan, J. P. Kreskovsky, and M. A. Stroscio, "Transport via the Liouville equation and moments of quantum distribution functions," *Solid-State Electronics*, vol. 36, pp. 1697–1709, 1993.

[5] C. L. Gardner, "The quantum hydrodynamic model for semiconductor devices," *SIAM Journal on Applied Mathematics*, vol. 54, pp. 409–427, 1994.

[6] F. Odeh and E. Thomann, "On the well-posedness of the two-dimensional hydrodynamic model for semiconductor devices," *COMPEL*, vol. 9, pp. 45–47, 1990.

[7] H. L. Grubin and J. P. Kreskovsky, "Quantum moment balance equations and resonant tunnelling structures," *Solid-State Electronics*, vol. 32, pp. 1071–1075, 1989.

[8] R. P. Feynman, *Statistical Mechanics: A Set of Lectures*. Reading, Massachusetts: W. A. Benjamin, 1972.

[9] See http://www.raytheon.com/rsc/ses/spr/spr_nan/nan_nem.htm.

[10] R. K. Lake, G. Klimeck, R. C. Bowen, and D. Jovanovic, "Single and multiband modeling of quantum electron transport through layered semiconductor devices," *Journal of Applied Physics*, vol. 81, pp. 7845–7869, 1997.

[11] R. K. Lake, G. Klimeck, R. C. Bowen, D. Jovanovic, D. K. Blanks, and M. Swaminathan, "Quantum transport with band-structure and Schottky contacts," *Physica Status Solidi B*, vol. 204, pp. 354–357, 1997.

[12] G. Klimeck, R. K. Lake, R. C. Bowen, W. R. Frensley, and T. S. Moise, "Quantum device simulation with a generalized tunneling formula," *Applied Physics Letters*, vol. 67, pp. 2539–2541, 1995.

[13] G. Klimeck, T. Boykin, R. C. Bowen, R. K. Lake, D. K. Blanks, T. S. Moise, Y. C. Kao, and W. R. Frensley, in *1997 55th Annual Device Research Conference Digest*, p. 92. IEEE, 1997.

[14] R. C. Bowen, G. Klimeck, R. K. Lake, W. R. Frensley, T. S. Moise, "Quantitative simulation of a resonant tunneling diode," *Journal of Applied Physics*, vol. 81, pp. 3207–3213, 1997.

[15] R. K. Lake, G. Klimeck, R. C. Bowen, C. Fernando, T. S. Moise, Y. C. Kao, "Interface roughness, polar optical phonons, and the valley current of a resonant tunneling diode," *Superlattices and Microstructures*, vol. 20, pp. 279–285, 1996.

[16] R. K. Lake, G. Klimeck, and D. K. Blanks, "Interface roughness and polar optical phonon scattering in $In_{0.53}Ga_{0.47}As$/AlAs/InAs RTDs," *Semiconductor Science and Technology*, vol. 13, pp. A163–A164, 1998.

[17] G. Klimeck, R. K. Lake, and D. K. Blanks, "Role of interface roughness scattering in self-consistent resonant-tunneling-diode simulations," *Physical Review B*, vol. 58, pp. 7279–7285, 1998.

Figure Captions

Figure 1: Current density in kiloamps/cm^2 vs. voltage comparing the smooth QHD (blue) and (one band one effective mass) NEMO (dotted magenta) models.

Figure 2: Current density in kiloamps/cm^2 vs. voltage for various NEMO models: one band one effective mass (dotted magenta), and from the right peak to the left peak, one band two effective masses (cyan), two bands two effective masses (red), ten bands two effective mass (blue).

Figure 3: Smooth QHD simulation of electron temperature in eV in the RTD. x is in 100 nanometers.

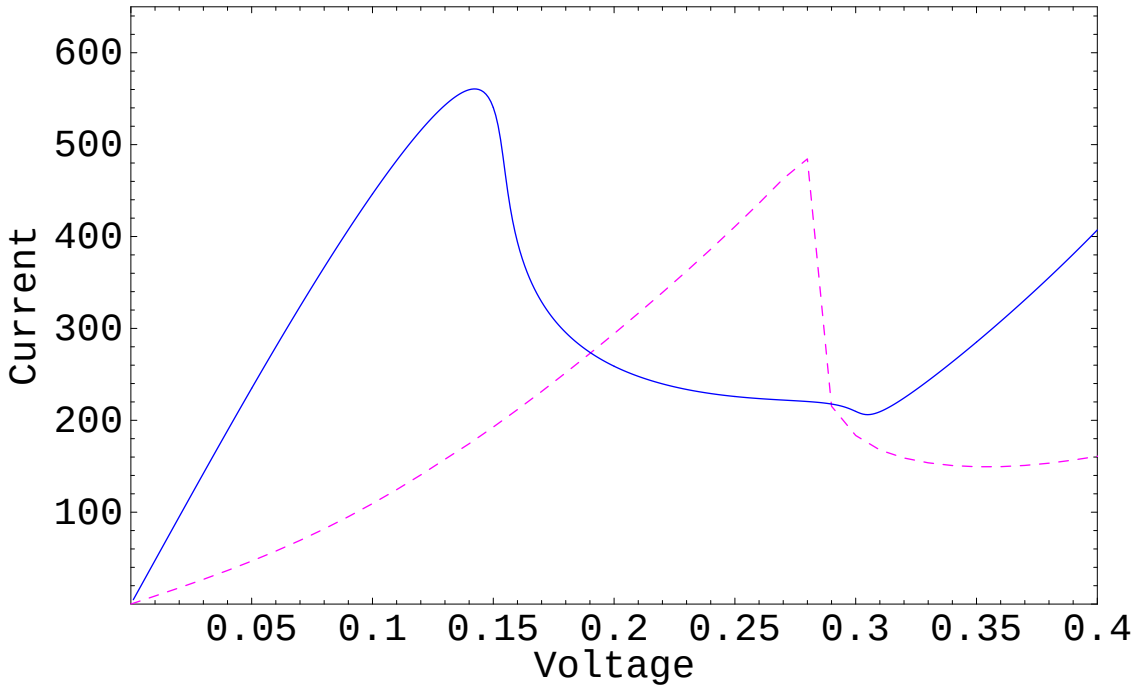

Figure 1: Current density in kiloamps/cm^2 vs. voltage comparing the smooth QHD (blue) and (one band one effective mass) NEMO (dotted magenta) models.

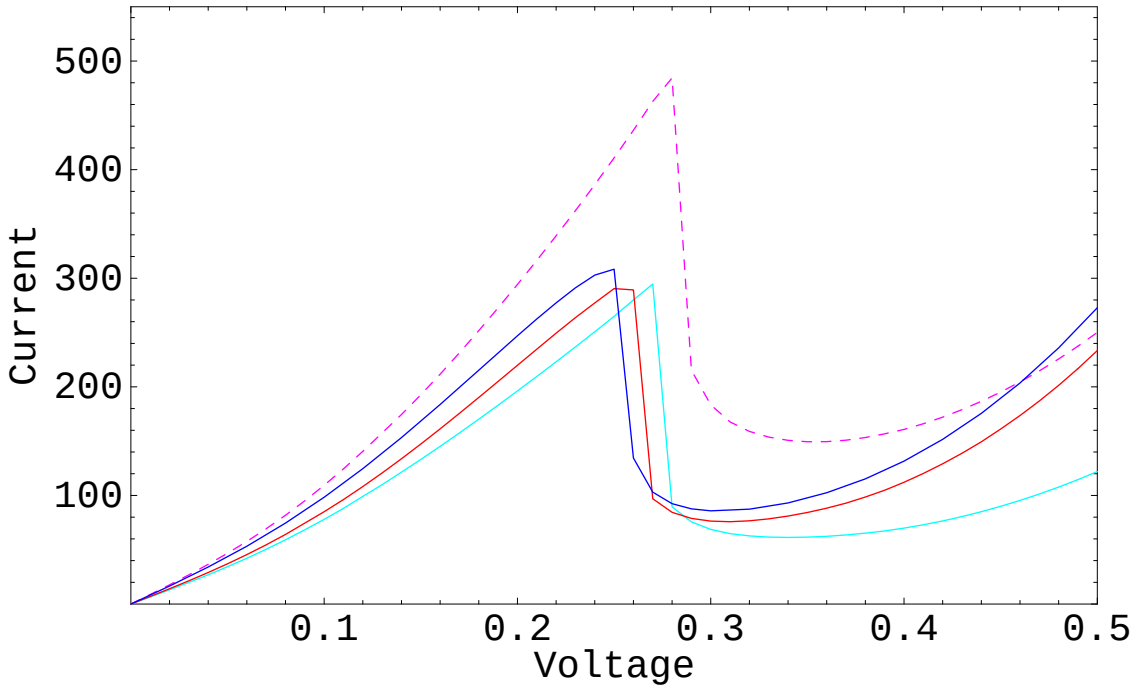

Figure 2: Current density in kiloamps/cm^2 vs. voltage for various NEMO models: one band one effective mass (dotted magenta), and from the right peak to the left peak, one band two effective masses (cyan), two bands two effective masses (red), ten bands two effective mass (blue).

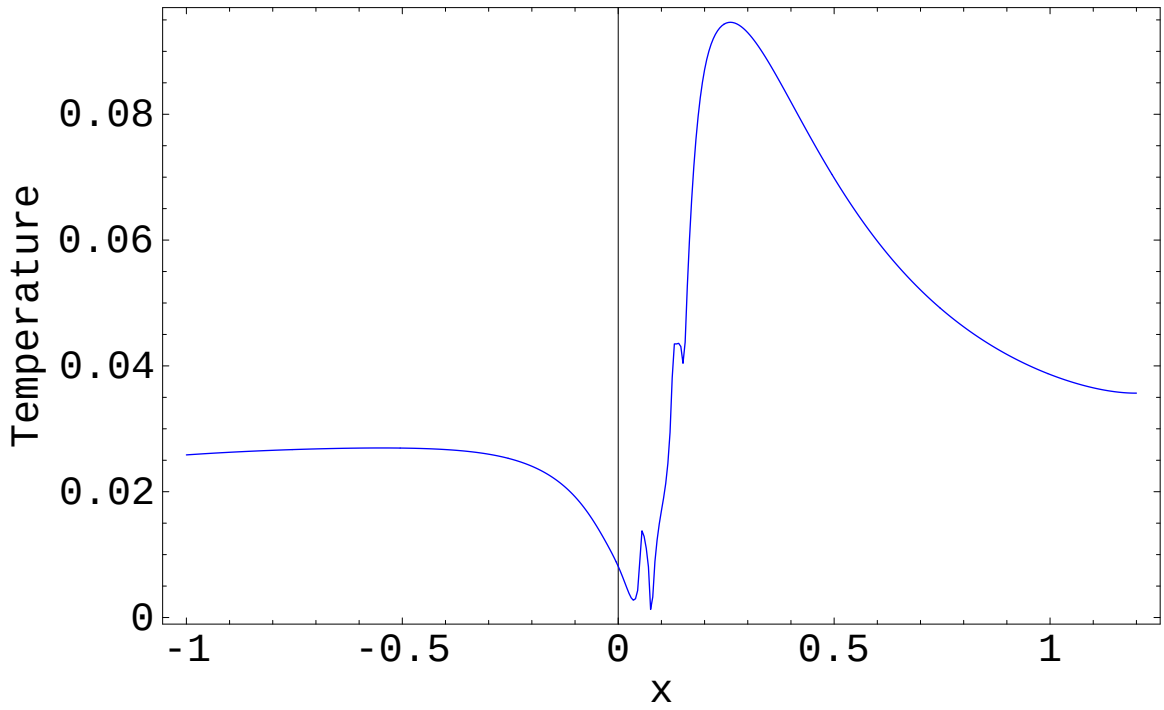

Figure 3: Smooth QHD simulation of electron temperature in eV in the RTD. x is in 100 nanometers.